Numerical study of long-time dynamics and ergodic-nonergodic transitions in dense simple fluids

David D. McCowan
The James Franck Institute and the Department of Physics, The University of Chicago, Chicago, Illinois 60637, USA
(Received 4 November 2014; published 6 August 2015)

Since the mid-1980s, mode-coupling theory (MCT) has been the *de facto* theoretic description of dense fluids and the transition from the fluid state to the glassy state. MCT, however, is limited by the approximations used in its construction and lacks an unambiguous mechanism to institute corrections. We use recent results from a new theoretical framework—developed from first principles via a self-consistent perturbation expansion in terms of an effective two-body potential—to numerically explore the kinetics of systems of classical particles, specifically hard spheres governed by Smoluchowski dynamics. We present here a full solution for such a system to the kinetic equation governing the density-density time correlation function and show that the function exhibits the characteristic two-step decay of supercooled fluids and an ergodic-nonergodic transition to a dynamically arrested state. Unlike many previous numerical studies—and in stark contrast to experiment—we have access to the full time and wave-number range of the correlation function with great precision and are able to track the solution unprecedentedly close to the transition, covering nearly 15 decades in scaled time. Using asymptotic approximation techniques analogous to those developed for MCT, we fit the solution to predicted forms and extract critical parameters. We find complete qualitative agreement with known glassy behavior (e.g. power-law divergence of the α-relaxation time scale in the ergodic phase and square-root growth of the glass form factors in the nonergodic phase), as well as some limited quantitative agreement [e.g. the transition at packing fraction $\eta^* = 0.60149761(10)$], consistent with previous static solutions under this theory and with comparable colloidal suspension experiments. However, most importantly, we establish that this new theory is able to reproduce the salient features seen in other theories, experiments, and simulations but has the advantages of being derived from first principles and possessing a clear mechanism for making systematic corrections.

DOI: 10.1103/PhysRevE.92.022107 PACS number(s): 05.70.Ln, 64.70.qj, 64.70.pm

I. INTRODUCTION

It is possible to compress or cool a fluid beyond the freezing point where it can crystalize into a solid and instead form a supercooled liquid or, eventually, a glass. As one approaches this glassy state, the dense fluid shows several features unique to this transition: The relaxation dynamics slow, the structure arrests, and a disordered nonequilibrium state emerges [1–4]. This glass transition is seen in a wide variety of fluids from complex molecular liquids [5–13] to simple colloidal suspensions [14–17].

When studying liquids and the transition from liquid to glass, the natural quantity to monitor is the density-density time correlation function,

$$G_{\rho\rho}(q,t) = \langle \delta\rho(\mathbf{q},t)\delta\rho(-\mathbf{q},0)\rangle, \tag{1}$$

where $\mathbf{q}$ is wave number, t is time, and $\delta\rho(\mathbf{q},t)$ is the particle density fluctuation, and the angle brackets represent the canonical ensemble average. This function captures the relaxation of the system away from the static structure factor $S(q) = G_{\rho\rho}(q,t=0)$ which characterizes the equilibrium static state.

In a dilute liquid, this function decays exponentially with time, but as one approaches the liquid-glass transition, there is a significant slowing down and a two-step decay emerges; at intermediate times the system remains nearly stationary, forming a plateau which can extend decades in time before finally relaxing to zero. The relaxation into and out of the extended plateau is called the β relaxation and the eventual relaxation out of the plateau and to zero is called the α relaxation. The time scales associated with these two dynamic regimes are τ_β and τ_α, respectively, and both diverge at the transition, leaving the intermediate structure factor unable to relax beyond the plateau; such a system is nonergodic and the ability of particles to diffuse through the whole of the system is halted.

This dynamic arrest appears in the long-time limit of the intermediate structure factor as a discontinuous jump from zero to the fixed plateau amplitude. In terms of the normalized correlator $F(q,t) = G_{\rho\rho}(q,t)/S(q)$, this limit is called the glass form factor, the plateau, or the nonergodicity factor:

$$\lim_{t\to\infty} F(q,t) = f_q \geqslant 0. \tag{2}$$

One of the first successful models of the glass transition was mode-coupling theory (MCT), introduced in the 1980s by Leutheusser and Goetze [18–21]. MCT begins with a generalized Langevin equation (or kinetic equation) for generic correlation function $C(t)$ of the form

$$\frac{\partial^2 C(q,t)}{\partial t^2} = -\Omega_q^2 C(q,t) - \int_0^t ds\, K(q,t-s)\frac{\partial C(q,s)}{\partial s}, \tag{3}$$

where $K(q,t)$ is the so-called memory function and Ω_q^2 is a time-independent quantity that depends on the nature of the correlation function $C(q,t)$ [22,23]. In the case where one studies the density-density time correlation function, the so-called mode-coupling approximation [4] gives rise to a memory function of the form

$$K(q,t) = \frac{1}{2}\int \frac{d^d\mathbf{k}}{(2\pi)^d} M^2(\mathbf{q},\mathbf{k}) G_{\rho\rho}(k,t) G_{\rho\rho}(|\mathbf{q}-\mathbf{k}|,t), \tag{4}$$

where

$$M^2(\mathbf{q},\mathbf{k}) = \frac{\rho}{q^2}[\hat{\mathbf{q}}\cdot\mathbf{k}V(k) + \hat{\mathbf{q}}\cdot|\mathbf{q}-\mathbf{k}|V(|\mathbf{q}-\mathbf{k}|)]^2 \tag{5}$$

is the vertex function, $V(q)$ is the pair-wise potential, and ρ is the average particle density. This approximation is not rigorously justified, but solutions to the kinetic equation nonetheless show the two-step decay for dense fluids and predict an ergodic-nonergodic transition at finite density.

Mode-coupling theory has undeniably had a number of successes. In addition to giving the correct qualitative form for the two-step decay, MCT makes remarkable predictions about power-law relaxation into and out of the plateau in the β regime as well as diverging time scales that have held up to experimental verification in weakly supercooled systems and hard-sphere systems. The MCT predictions for the nonergodicity factor f_q have also matched measured quantities [4,24–27].

MCT, however, also has a number of shortcomings. Most pointedly, MCT does not accurately predict some of the parameters of the transition, including the transition temperatures and densities; is not derived from first principles; and has no clear method for controlled improvements [22,28]. For this reason, there is great interest in a new theory which improves over MCT. There have been a number of previous attempts (see Sec. IV for more on this point), but we here expand on the promising recent theory of Mazenko [29–33] and use it to develop the full dynamic results in a model system of hard spheres obeying Smoluchowski dynamics (SD).

The theory—a field-theoretic approach that derives the intermediate structure factor (and other correlation functions) in a self-consistent perturbation expansion in the pairwise potential—yields a kinetic equation and memory function very similar to that of MCT at second order in the potential expansion [34] and produces all the expected features near the ergodic-nonergodic transition. The full numerical solution shows a two-step relaxation, diverging length scales τ_α and τ_β, power-law decay into and out of the plateau in the β regime, and scaling of the amplitudes of the nonergodicity factor, f_q [35]. The value we find for the transition density is in rough agreement with relevant theory, experiment, and simulation (unlike MCT's) [36,37], and our power-law decays obey the predicted forms, though with parameter values that differ from those seen elsewhere for hard spheres [25,36,38]. Likewise, our nonergodicity factors f_q show similarity to, but not quantitative agreement with, measured results [25,38].

The structure of this paper is as follows. In Sec. II, we introduce the theory and motivate the governing equations. While the connection to the work of mode-coupling theory occurs at second order in the potential expansion, we very briefly summarize results at zeroth and first orders in order to show how new physics are introduced order by order. In addition to the governing equations, we also remind the reader of the asymptotic analysis which makes predictions for the critical dynamics near the transition.

In Sec. III, we define the system we study—hard spheres obeying Smoluchowski dynamics—and walk through the numerical solution to the kinetic equation. We highlight features of the intermediate structure factor at different packing fraction densities and wave numbers and find the two-step decay in the ergodic phase giving way to a clear transition to the nonergodic phase. Through fits of the data, we explore the divergence of the α- and β-relaxation times and extract values for the critical power-law exponents. Finally, we compare these results to mode-coupling theory as well as other theories, experiments, and simulation results in Sec. IV.

Unlike many previous numerical studies—and in stark contrast to experiment—this study yields the full time and wave-number range of the correlation function with great precision. As such, we are able to track the solution unprecedentedly close to the transition, covering nearly 15 decades of scaled time and having access to very detailed data against which to fit and test predicted forms.

It is again worth stressing that this work is a numerical solution to the full dynamics near an ergodic-nonergodic transition, but importantly one derived from a theory outside mode-coupling theory. While there are some quantitative disagreements with other theories, experiments, and simulations at the approximation order presented here, the qualitative behavior shows the characteristic features of the glass transition. Most importantly, this theory is the product of a well-motivated and self-consistent perturbation expansion and therefore can be corrected by continuing the expansion in potential to higher order. It remains to be seen whether these corrections bring the quantitative results into better agreement with other literature, but there is no denying that the mere ability to apply well-defined corrections opens this technique up as a new and promising tool for studying supercooled fluids.

II. THEORY

A fundamental theory of statistical particle dynamics that unifies kinetic theory, Brownian motion, and field theory techniques was developed in Ref. [29] for Smoluchowski dynamics and extended in Ref. [31] to Newtonian dynamics (ND). Here we review the main points.

A. Fundamental theory of statistical particle dynamics

Imagine a system of N particles of mass m located at positions $R_i(t)$ and possessing momenta $P_i(t)$. Such particles interact via a pair potential

$$U = \frac{1}{2}\sum_{i\neq j} V(R_i - R_j), \tag{6}$$

which leads to a force

$$F_i = -\nabla_i U. \tag{7}$$

Under Newtonian dynamics, the equations of motion are

$$m\dot{R}_i = P_i \quad \text{and} \quad \dot{P}_i = F_i. \tag{8}$$

If, however, the particles interact with a thermal bath such that the individual momenta are quickly dissipated, the system can instead by described by simpler Smoluchowski dynamics. In this case, we have only the Langevin equation given by

$$\dot{R}_i = DF_i + \eta_i, \tag{9}$$

where D is the diffusion coefficient and $\eta_i(t)$ is Gaussian-distributed random noise with zero mean

$$\langle \eta_i(t)\rangle = 0 \tag{10}$$

and variance proportional to temperature

$$\langle \eta_i(t)\eta_j(t')\rangle = 2D\beta^{-1}\delta_{ij}\delta(t-t'), \tag{11}$$

where $\beta^{-1} = k_B T$ and where the angle brackets here represent canonical ensemble averages [39].

We wish to move from these equations of motion to a field theory. One can form a Martin-Siggia-Rose (MSR) action [43,44] which leads to a grand-canonical partition function. For a set of core dynamical fields $\Phi = \{\Phi_\alpha\}$ which interact with each other through matrix $\sigma_{\alpha\beta}$, we have

$$Z_T = \sum_{N=0}^{\infty} \frac{\rho_0^N}{N!} \mathrm{Tr} e^{-A_I + H\cdot\Phi}, \tag{12}$$

where ρ_0 is the fugacity (or bare density) and where the interacting terms of the action are given by

$$A_I = \frac{1}{2} \sum_{\alpha\beta} \int d\mathbf{x}_1 dt_1 d\mathbf{x}_2 dt_2 \Phi_\alpha(\mathbf{x}_1,t_1)\sigma_{\alpha\beta}(\mathbf{x}_1,\mathbf{x}_2,t_1,t_2)\Phi_\beta(\mathbf{x}_2,t_2) \tag{13}$$

or, in shorthand,

$$A_I = \tfrac{1}{2}\Phi_\alpha(1)\sigma_{\alpha\beta}(12)\Phi_\beta(2), \tag{14}$$

such that repeated subscripts are summed over and repeated space and time arguments are integrated over. The noninteracting terms of the action, $A_0 = A - A_I$, and the initial conditions have been rolled into the trace and we allow for coupling to external fields $H = \{H_\alpha\}$ via a Zeeman-like term,

$$H_\alpha(1)\Phi_\alpha(1) = \sum_\alpha \int d\mathbf{x}_1 dt_1 H_\alpha(\mathbf{x}_1,t_1)\Phi_\alpha(\mathbf{x}_1,t_1). \tag{15}$$

Details of the development of the action and the trace are discussed more carefully in Ref. [29].

There are two essential physical fields which appear in the Hamiltonian and which therefore define what we will term the *core* problem. These two fields—the density $\rho(\mathbf{x},t)$ and the response field $B(\mathbf{x},t)$—must always be included,

$$\Phi(1) = \{\rho(\mathbf{x}_1,t_1), B(\mathbf{x}_1,t_1), \ldots\}, \tag{16}$$

and couple to each other via the interaction matrix,

$$\sigma_{\alpha\beta}(12) = V(\mathbf{x_1} - \mathbf{x_2})\delta(t_1 - t_2)[\delta_{\alpha\rho}\delta_{\beta B} + \delta_{\alpha B}\delta_{\beta\rho}], \tag{17}$$

where $V(\mathbf{x_1} - \mathbf{x_2})$ is the same pair potential defined above in Eq. (6) [45].

The density $\rho(\mathbf{x},t)$ is of the usual form for both types of dynamics,

$$\rho(\mathbf{x},t) = \sum_{i=1}^{N} \delta[\mathbf{x} - \mathbf{R}_i(t)]; \tag{18}$$

however, the response field $B(\mathbf{x},t)$ which emerges is unique to this theory and its form depends on whether one studies Newtonian or Smoluchowski dynamics. The response field B is key to the development of this theory and marks an important break with MSR tradition where the conjugate position and momenta fields themselves play a response role.

From the partition function, we may construct the generating functional

$$W[H] = \ln Z_T[H] \tag{19}$$

and form cumulants by taking successive functional derivatives with respect to the coupling field. The two-point cumulant, for example, is given by

$$G_{\alpha\beta}(\mathbf{x}_1,t_1;\mathbf{x}_2,t_2) = \langle \delta\Phi_\alpha \delta\Phi_\beta \rangle = \frac{\delta}{\delta H_\alpha}\frac{\delta}{\delta H_\beta} W[H] = \frac{\delta}{\delta H_\beta} G_\alpha. \tag{20}$$

Keeping the coupling fields can, for example, allow one to treat trapped or driven systems, but we will here only be concerned with the steady-state cumulants where all H_α are set to zero after taking the derivatives.

Though the above is exact, it is a formal development. In order to make traction, one must perform a series expansion to compute forms for the cumulants order by order. The key identity [29] is

$$G_\alpha = \mathrm{Tr}\phi_\alpha e^{H\cdot\phi + \Delta W[H]}, \tag{21}$$

where

$$\begin{aligned}\Delta W[H] = {} & \phi_\alpha(1)\sigma_{\alpha\beta}(12)G_\beta(2) \\ & + \tfrac{1}{2}\phi_\alpha(1)\phi_\beta(2)\sigma_{\alpha\gamma}(13)\sigma_{\beta\delta}(24)G_{\gamma\delta}(34) \\ & + \tfrac{1}{3!}\phi_\alpha(1)\phi_\beta(2)\phi_\gamma(3)\sigma_{\alpha\delta}(14)\sigma_{\beta\epsilon}(25)\sigma_{\gamma\zeta}(36) \\ & \times G_{\delta\epsilon\zeta}(456) + \ldots \end{aligned} \tag{22}$$

and where

$$\Phi_\alpha(\mathbf{x},t) = \sum_{i=1}^{N} \phi_i(\mathbf{x},t). \tag{23}$$

Each derivative brings down a factor of $\Delta W[H]$ which can be truncated to any order in the interaction matrix $\sigma_{\alpha\beta}(12) \sim V(\mathbf{x}_1 - \mathbf{x}_2)$. In this way, we have now cast the problem as a self-consistent perturbation expansion in the potential. Once one solves for the zeroth-order (i.e., noninteracting) cumulants—a nontrivial endeavor—higher orders are generated by turning the crank.

Finally, we define the vertex function (or matrix inverse) via Dyson's equation. For two-point quantities, this takes the form

$$\Gamma_{\alpha\mu}(13)G_{\mu\beta}(32) = \delta_{\alpha\beta}. \tag{24}$$

Importantly, n-point cumulants and vertices (regardless of dynamics) obey fluctuation-dissipation relations which hold both order by order in the expansion and for the full cumulant [32]. The most useful of these is the two-point cumulant fluctuation dissipation relation,

$$G_{\rho B}(12) = \theta(t_1 - t_2)\beta\frac{\partial}{\partial t_1} G_{\rho\rho}(12). \tag{25}$$

B. Zeroth- and first-order solutions

Full zeroth- and first-order results have been worked out for Smoluchowski and Newtonian dynamics elsewhere. As an example, in the Smoluchowski case the zeroth-order density-density cumulant is

$$G^{(0)}_{\rho\rho}(q,t) = \rho_0 e^{-Dq^2 t/\beta}, \tag{26}$$

while at first order we have

$$G^{(1)}_{\rho\rho}(q,t) = S(q)e^{-D\tilde{\rho}q^2 t/\beta S(q)}. \tag{27}$$

Here the static structure factor is given by

$$S(q) = \frac{\bar{\rho}}{1 + \bar{\rho}\beta V(q)}, \tag{28}$$

where the bare density ρ_0 is everywhere replaced by the first-order revised average density

$$\bar{\rho} = \frac{\rho_0}{1 + \rho_0 \beta V(q=0)}. \tag{29}$$

We see that that the decay of $G_{\rho\rho}(q,t)$ is exponential in both cases, but at first order the relaxation time is inversely proportional to the static structure factor leading to a slowing down near the first structure factor peaks. This is the well-known de Gennes narrowing form [46].

At this level of approximation, let us review how we can use these results in practice.

Our theory requires one input—a static structure factor $S(q)$—which is used by Eq. (28) to find the effective potential—also called the pseudopotential—$V(q)$. This in turn updates the density, Eq. (29), and yields the density-density correlation function, Eq. (27). Advanced or retarded response functions $G_{B\rho}(q,t)$ or $G_{\rho B}(q,t)$ can be found, if needed, through the fluctuation-dissipation relation, Eq. (25).

At first order, Eq. (28) is in the form of the static Ornstein-Zernike relation [47], and we can identify the effective interaction with $c_D(q)$, the physical direct correlation function, which is assumed to be known by other means [48,49]:

$$V(q) = -\beta^{-1} c_D(q). \tag{30}$$

We see, then, that any theoretical or experimentally measured structure factor $S(q)$ or direct correlation function $c_D(q)$ is sufficient to work out the full dynamic results. Already at first order in the perturbation we have a theory valid for low-density fluids and a clear mechanism for going further.

C. The kinetic equation and the memory function: Second-order solution

As we continue expanding in potential, we find that Dyson's equation in conjunction with the fluctuation-dissipation relation again gives rise to a kinetic equation governing the full dynamics of the intermediate structure factor, $G_{\rho\rho}(q,t)$. At second order, we have

$$\left[D_q \frac{\partial^2}{\partial t^2} - A_q \frac{\partial}{\partial t} - \beta^{-1} S^{-1}(q)\right] G_{\rho\rho}(q,t) = \int_0^t ds \beta K(q,t-s) \frac{\partial}{\partial s} G_{\rho\rho}(q,s), \tag{31}$$

where for Smoluchowski dynamics [30,34] we have

$$D_q^{(\mathrm{SD})} = 0, \text{ and } A_q^{(\mathrm{SD})} = \frac{1}{\bar{\rho} D q^2} \tag{32}$$

and for Newtonian dynamics [32,33] we have

$$D_q^{(\mathrm{ND})} = \frac{-m\beta}{\beta \bar{\rho} q^2} \text{ and } A_q^{(\mathrm{ND})} = 0, \tag{33}$$

where $\bar{\rho}$ is the density revised to second order and where $K(q,t) = -\Gamma_{BB}(q,t)$ is the memory function. These equations are structurally identical to the well-known form derived in MCT [4,24,26,27]; however, we can already see how this theory now allows one to continue computing the equation of state $\bar{\rho}$ and the memory function $K(q,t)$ to arbitrary order.

At this order, the effective potential $V(q)$ is the solution to the equation for the static structure factor

$$S(q) = \frac{1}{1 + V(q) - M(q)}, \tag{34}$$

where

$$M(q) = \frac{\pi}{12\eta} \int \frac{d^d\mathbf{k}}{(2\pi)^d} V(k) S(k) V(|\mathbf{q}-\mathbf{k}|) S(|\mathbf{q}-\mathbf{k}|), \tag{35}$$

and the average density $\bar{\rho}$ is found via

$$\rho_0 = \bar{\rho}\left[V(q=0) - \frac{1}{2\bar{\rho}} \int \frac{d^d\mathbf{k}}{(2\pi)^d} V^2(k) S(k)\right]. \tag{36}$$

Normalizing the intermediate structure factor,

$$F(q,t) = G_{\rho\rho}(q,t)/S(q), \tag{37}$$

switching from density $\bar{\rho}$ to packing fraction, $\eta = \pi\bar{\rho}\sigma^3/6$, and moving to all variables to dimensionless quantities, we have

$$\frac{\partial}{\partial t} F(q,t) = -q^2 S^{-1}(q) F(q,t) + q^2 \int_0^t ds K(q,t-s) \frac{\partial}{\partial s} F(q,s) \tag{38}$$

for the Smoluchowski case and

$$\frac{\partial^2}{\partial t^2} F(q,t) = -q^2 S^{-1}(q) F(q,t) + q^2 \int_0^t ds K(q,t-s) \frac{\partial}{\partial s} F(q,s) \tag{39}$$

for the Newtonian case.

The full memory function was derived to second order in the potential in Ref. [34] for Smoluchowski dynamics and in Ref. [32] for Newtonian dynamics (in the large-wavelength limit only). As discussed there, correcting the vertex functions to higher order will add derivative terms which influence short-time but not long-time dynamics; consequently, we will use their zeroth-order approximations in this work to simplify the equations.

Summarizing here, the memory function is

$$K(q,t) = K^{(s)}(q,t) + K^{(c)}(q,t), \tag{40}$$

where the self-contribution is given by

$$K^{(s)}(q,t) = \frac{\pi}{12\eta} \int \frac{d^d\mathbf{k}}{(2\pi)^d} [V^2(k) S(k) \tilde{F}(k,t) F^{(0)}(|\mathbf{q}-\mathbf{k}|,t) + V^2(|\mathbf{q}-\mathbf{k}|) S(|\mathbf{q}-\mathbf{k}|) F^{(0)}(k,t) \tilde{F}(|\mathbf{q}-\mathbf{k}|,t)] \tag{41}$$

and where the collective contribution is given by

$$K^{(c)}(q,t) = \frac{\pi}{12\eta} \int \frac{d^d\mathbf{k}}{(2\pi)^d} V(k) S(k) V(|\mathbf{q}-\mathbf{k}|) S(|\mathbf{q}-\mathbf{k}|) \times \bar{F}(k,t) \bar{F}(|\mathbf{q}-\mathbf{k}|,t). \tag{42}$$

Note that these terms do not depend on the full propagator $F(q,t)$ but on the dressed propagators $\bar{F}(q,t)$ and $\tilde{F}(q,t)$,

$$\bar{F}(q,t) = \bar{G}_{\rho\rho}(q,t)/\bar{G}_{\rho\rho}(q,t=0), \tag{43}$$

$$\tilde{F}(q,t) = \tilde{G}_{\rho\rho}(q,t)/\tilde{G}_{\rho\rho}(q,t=0), \tag{44}$$

and the noninteracting propagator

$$F^{(0)}(q,t) = G^{(0)}_{\rho\rho}(q,t)/G^{(0)}_{\rho\rho}(q,t=0), \tag{45}$$

which will decay to zero at long times regardless of the dynamics.

The dressed propagators arise naturally in the derivation and behave much like the normal correlation function, $F(q,t)$. Most importantly, the dressed propagators $\bar{G}_{\alpha\beta}$ and $\tilde{G}_{\alpha\beta}$ are themselves subject to fluctuation-dissipation relations.

More complete information about the dressed propagators is given in Appendix, but for our discussion here it suffices to say that both functions decay quicker than $F(q,t)$ at short times but approach the full correlation function at long times:

$$\bar{F}(q,t) \to F(q,t),\ t \gg 1, \tag{46}$$

$$\tilde{F}(q,t) \to F(q,t),\ t \gg 1. \tag{47}$$

In fact, we can use the long-time limits to form an approximate memory function

$$K^{(\mathrm{LT})}(q,t) = \frac{\pi}{12\eta}\int \frac{d^d\mathbf{k}}{(2\pi)^d} V(k)S(k)V(|\mathbf{q}-\mathbf{k}|)S(|\mathbf{q}-\mathbf{k}|) \times F(k,t)F(|\mathbf{q}-\mathbf{k}|,t), \tag{48}$$

where we have replaced $\bar{F}(q,t)$ and $\tilde{F}(q,t)$ with $F(q,t)$ and where we have dropped the self-contribution which will be subdominant to the collective contribution at long time due to its dependence on the noninteracting cumulant $F^{(0)}(q,t)$.

This long-time approximate form is strikingly similar to the mode-coupling theory memory function, Eq. (4); it is quadratic in the potential and quadratic in the density-density time correlation function, though, importantly, Eq. (48) has been derived from first principles by a controlled, systematic approximation.

D. Static solution at second-order

As shown in Ref. [35], we can write down an equation for the nonergodicity factor, f_q, in terms of static quantities only:

$$\frac{f_q}{1-f_q} = \mathcal{F}[f_q], \tag{49}$$

where

$$\mathcal{F}[f_q] = \frac{\pi}{12\eta}\int \frac{d^d\mathbf{k}}{(2\pi)^d} V(k)S(k)V(|\mathbf{q}-\mathbf{k}|)S(|\mathbf{q}-\mathbf{k}|) f_k f_{|\mathbf{q}-\mathbf{k}|}. \tag{50}$$

We may rearrange to find

$$f_q = \frac{\mathcal{F}[f_Q]}{1+\mathcal{F}[f_Q]}, \tag{51}$$

which can be solved by iteration.

In the liquid phase, only the trivial solution $f_q = 0$ for all q is supported, but at the transition density, the solution bifurcates, allowing the possibility of a discontinuous jump to a second, positive result.

E. Asymptotic expansion prediction

One of the most important predictions of mode-coupling theory is that the relaxation of the system through the β regime is governed by a set of master equations which predict power-law decay into and out of the plateau. In addition, the exponents are predicted to be universal properties of the system and the time scales associated with the α and β regimes themselves are predicted to diverge as power laws.

The theory developed in this paper can be treated identically as in MCT [35]; our system is expected to display the same power-law decay structure, though the values of the associated parameters may differ. We summarize the predicted forms here and point the reader to Refs. [26,27] for more details.

Let us change from temperature T (or packing fraction η) to the system-independent separation parameter $\epsilon = (T^* - T)/T^*$ (or $\epsilon = (\eta - \eta*)/\eta^*$) where T^* (or η^*) is the location of the ergodic-nonergodic transition.

In the β regime, the correlation function is modeled as a small deviation from the plateau of *critical amplitude* h_q. In the nonergodic phase ($\epsilon \geqslant 0$), we have

$$F(q,t) - f_q^* = h_q \begin{cases} (t/\tau_0)^{-a} & : \tau_0 \ll t \ll \tau_\beta; \epsilon \geqslant 0 \\ \sqrt{\epsilon/(1-\lambda)} & : t \to \infty; \epsilon \geqslant 0, \end{cases} \tag{52}$$

and in the ergodic phase ($\epsilon < 0$),

$$F(q,t) - f_q^* = h_q \begin{cases} (t/\tau_0)^{-a} & : \tau_0 \ll t \ll \tau_\beta; \epsilon < 0 \\ -(t/\tau_\alpha)^b & : \tau_\beta \ll t \ll \tau_\alpha; \epsilon < 0. \end{cases} \tag{53}$$

Here $0 < a < 1/2$ is the first critical exponent, $0 < b < 1$ is the second critical exponent, and λ is the exponent parameter relating the two,

$$\lambda = \frac{\Gamma(1-a)^2}{\Gamma(1-2a)} = \frac{\Gamma(1+b)^2}{\Gamma(1+2b)}, \tag{54}$$

which is constrained to be $1/2 \leqslant \lambda \leqslant 1$. The two time scales diverge as

$$\tau_\beta = \frac{\tau_0}{|\epsilon|^{1/2a}} \quad \text{and} \quad \tau_\alpha = \frac{\tau_0}{|\epsilon|^\gamma}, \tag{55}$$

where $\gamma = 1/2a + 1/2b$.

We see that in the approach to the plateau, both the ergodic and nonergodic systems behave identically; it is only at long times when the system decays out of the plateau (or not) that a distinction can be made.

In the ergodic phase, no simple model for the final relaxation to zero through the α regime falls out of the asymptotic expansion. The initial decay out of the plateau is termed the von Schweidler relaxation and one might assume this form would hold all the way to zero. It is believed, however, that there is a complex interplay of relaxation on different length scales such that the power laws at different wave numbers become superimposed [50]. Experimentally, this so-called time-temperature superposition is remarkably well modeled

as a stretched-exponential form [60,61],

$$F(q,t) = A_q \exp[-(t/\tau_q)^{\beta_q}], \tag{56}$$

where $\beta_q \leqslant 1$ and where $A_q \leqslant f_q$ allows for the fact that the exponential behavior need not take over until some time after the initial decay away from the plateau. The effective time constant τ_q defined here is wave-number dependent (due to the mixing described above) but will be proportional to and of the same order as τ_α. Scaling time in the intermediate structure factor by τ_α causes the long-time behavior of $F(q,t)$ at all densities near the transition to collapse onto one curve from the von Scheweidler decay out of the β regime through the whole of the α regime.

III. SOLUTION FOR HARD SPHERES OBEYING SMOLUCHOWSKI DYNAMICS

A. Defining the system

To this point, we have kept the discussion general as this theory is applicable to a wide variety of systems. However, let us now look at a concrete example and solve the kinetic equation for a system of hard spheres obeying Smoluchowski dynamics. We choose this system first as a simple, but nontrivial, system that shows all of the dynamic features predicted thus far. In addition, working with hard spheres allows us a straightforward comparison with simulation and experiment; as will be discussed in later sections, an appropriate analog to hard spheres is a colloid suspension [62] and there is detailed work on such systems against which we may compare our results [14–17,25,36].

Recall that the theory requires one input—a static structure factor. As is common with hard spheres, we will use the Ornstein-Zernike equation for the static structure factor [47] with the Percus-Yevick approximation for the direct correlation function, $c_D(q) = -V(q)$ [48,49]. Note that in the case of hard spheres, temperature drops out; the only control parameter is the packing fraction density, η.

We may update our effective potential to second order through Eq. (34). The effect of including higher-order terms in the pseudopotential, however, causes only a moderate change in the position of the transition as determined by the static solution. While a full investigation of this effect should eventually be done, we will here stick with the first-order solution; at this order, both $S(q)$ and $V(q)$ match the commonly-used Percus-Yevick forms, making comparison to other work simpler [63].

B. Numerical solution

The kinetic equation, Eq. (38), does not have an analytic solution for general $S(q)$, so we must instead solve it numerically to find the full function $F(q,t) = G_{\rho\rho}(q,t)/S(q)$ subject to the initial conditions $F(q,t=0) = 1$ and $\partial F(q,t)/\partial t|_{t=0} = 0$.

Our solution uses the numerical algorithm developed by Fuchs, *et al.* [64,65]. The density-density correlation function and memory function are discretized in time and wave number and the solution is advanced in steps from the initial conditions out to long times. Rather than proceed uniformly, though, this algorithm has a time step size which doubles after a fixed number of steps. This allows one to use small intervals at early times (where accuracy is key) and larger intervals at late times (where speed is key). This adaptive routine is essential for computing over the many decades of decay necessary here. No artificial large wave-number cutoff is needed as the correlation and memory functions approach zero at large wave numbers sufficiently quickly.

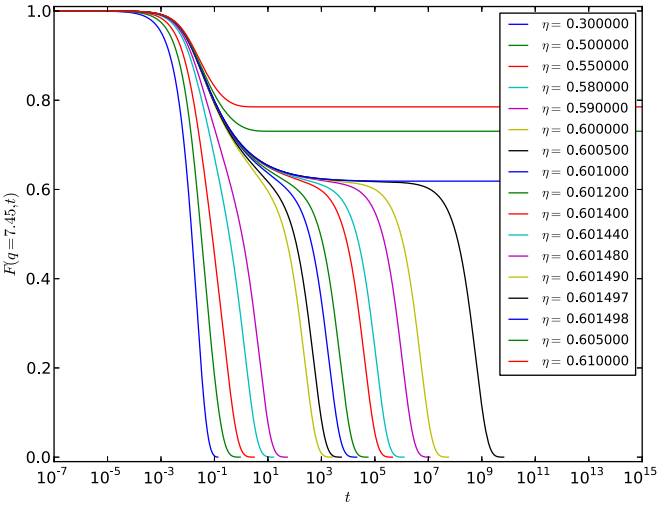

FIG. 1. (Color online) $F(q,t)$ is shown as a function of time at fixed wave number $q = 7.45$ near the first structure factor maximum for select values of packing fraction η; the value of η increases curve to curve as one moves from the leftmost curve ($\eta = 0.30$) to the rightmost curve ($\eta = 0.61$). As the density increases toward the transition density of $\eta^* = 0.60149761$ from values below, there is a dramatic slowdown with the system remaining trapped near the plateau in the β regime over many decades. Above the transition, the system becomes nonergodic and remains locked in the plateau at long times.

First, we consider the solution using the long-time limit form of the memory function, Eq. (48). (Select densities are plotted in Fig. 1 at fixed wave number.) The intermediate structure factor shows a slower relaxation compared to both the zeroth- and first-order solutions at all densities, and the full two-step decay emerges as the packing fraction rises above $\eta \approx 0.60$. The plateau which appears rapidly grows longer with increasing density until we find the transition to a nonergodic phase for $\eta > 0.601497$. The densities probed here represent decay over more than a dozen decades of time.

Next, we may repeat our solution but with the more complete, no-vertex correction form of the second-order memory function given in Eq. (40). In this case, we must keep track not only of $F(q,t)$ but also the dressed propagators, $\bar{F}(q,t)$ and $\tilde{F}(q,t)$. As discussed in the theory section, both of these functions decay faster than $F(q,t)$ at short times but tend toward the undressed $F(q,t)$ at long times. (Plots of the dressed propagators are shown in Fig. 9 in Appendix) The solution in this case is identical except for an overall shift in the short time scale, $\tau_0 \to \tau_0'$; the two-step decay has the same form and the ergodic-nonergodic transition occurs at the same packing fraction. We will therefore restrict numerical results discussed for the remainder of this work only to the solution using the long-time form of the memory function.

Numerically solving the kinetic equation for this system represents an important step in the study of the glass-transition problem: This theory is the first outside of mode-coupling theory to show a full dynamic solution with both the two-step decay and an ergodic-nonergodic transition. As will be shown in the following section, this solution reproduces features seen in experiment and simulation and exhibits functional forms and scalings of the same type as MCT. It bares repeating, however, that this form of the theory and the assumptions which go into the numerical solution are better motivated than those of MCT. Additionally, the clear mechanism for instituting corrections will allow future solutions to be carried out at higher order in the expansion of the effective potential, exploring how the physics evolve order by order.

C. Fitting

Let us fit our results in order to extract values of the critical exponents and test the predicted scaling laws. The chief difficulty in performing these fits comes from determining the regions of the data where each predicted form is applicable; several of the parameters change quickly with modest adjustments to the fit domain. This is a well-known challenge within MCT [25,38] and for fitting power law forms in general where one typically requires many decades of data to be confident in the results.

Our approach, therefore, will not be to attempt a direct fit to $F(q,t)$ on our first pass but instead to deduce the values of the critical amplitude and critical exponents indirectly; a fit of τ_α as a function of density will yield critical exponent γ which can be used to find a and b. On second pass, we will then return to the naïve approach of direct fitting and show that results are consistent despite having only a few decades of data to work with in each domain.

1. The nonergodicity factor, f_q

First, let us look at the nonergodicity factor f_q and investigate how it scales with density.

Recall that f_q had previously been found using the static equation, Eq. (51) [35]. We expect that extracting the nonergodicity factor directly from our results as the long-time limit,

$$\lim_{t\to\infty} F(q,t) = f_q, \tag{57}$$

should yield the same results and in fact find no difference, verifying the reliability of the static solution. The nonergodicity factor at the critical density is shown in Fig. 2.

From Eq. (52), we have that at fixed q the nonergodicity factor scales with density as

$$f_q = f_q^* + h_q\sqrt{\frac{\eta-\eta^*}{\eta^*(1-\lambda)}}. \tag{58}$$

We fit this form over a wide range of wave numbers and plot select results in Fig. 3. Each fit yields a comparable value for the transition density of $\eta^* = 0.60149761(10)$ where the uncertainty comes from the small spread in values over the different fits [66]. Coupling these fits with our determination of λ in the next section, we extract the critical amplitude h_q which is plotted in Fig. 4.

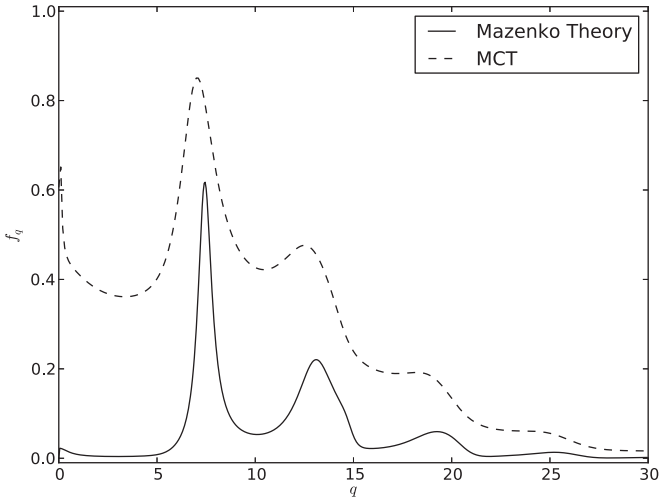

FIG. 2. A plot of the nonergodicity factor f_q at the transition density $\eta^* = 0.60149761$ along with the MCT result computed at the MCT critical density $\eta^* = 0.515$. Qualitatively, the two plots looks similar, though there are obvious quantitative differences. Both functions peak at the same wave numbers as the static structure factor.

2. The α-relaxation time scale, $\tau_\alpha \propto \tau_q$

Next, we look at the α relaxation in the ergodic phase. As described above, one can scale the time variable of the intermediate structure factor by τ_α and collapse the function onto one master curve at long times.

While it is possible to extract τ_α from the data, we need not find that time specifically. Any time proportional to τ_α will show the same scaling and τ_q—the effective time constant of the stretched exponential fit of the α relaxation, Eq. (56)—is

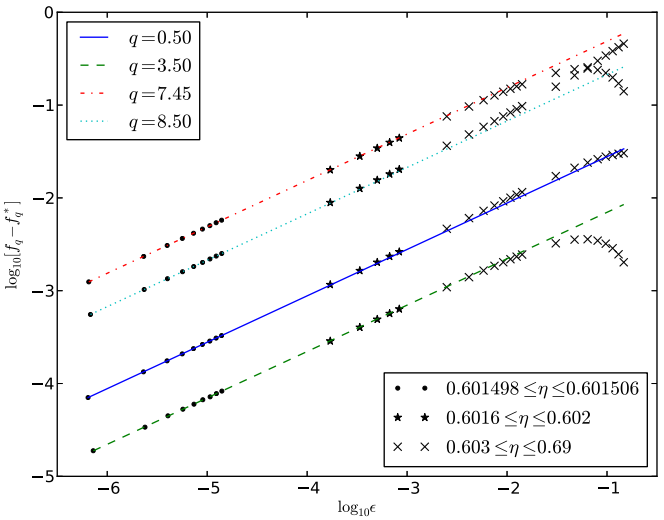

FIG. 3. (Color online) Fits of the nonergodicity factor to Eq. (58) for select values of wave number are plotted on a log-log scale such that each curve is linear with slope 1/2. Only points for $\eta \leqslant 0.601506$ ($\epsilon \leqslant 2\times10^{-5}$) were used in the fit, though the fit function is extended through $\eta = 0.69$ to show where the data depart from the model. For all wave numbers, agreement is good to $\eta \approx 0.602$ ($\epsilon \approx 10^{-3}$).

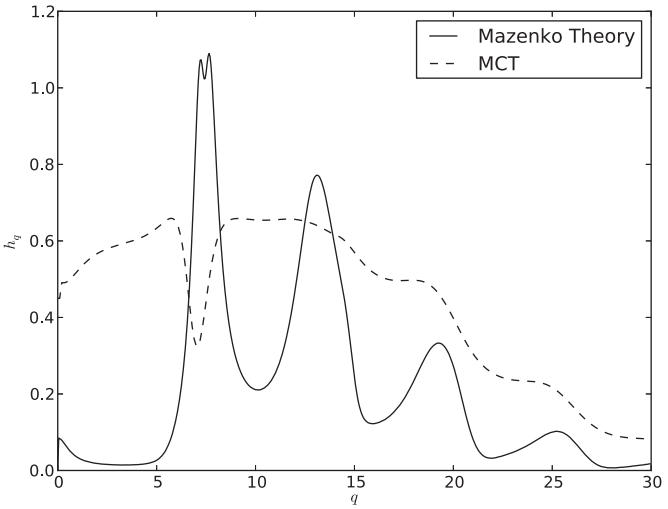

FIG. 4. The critical amplitude h_q is computed from from fits to the nonergodicity factor, Eq. (58), and plotted alongside the MCT prediction. While both show the characteristic dip near the first structure factor, there is less overall agreement than was seen between f_q functions in Fig. 2.

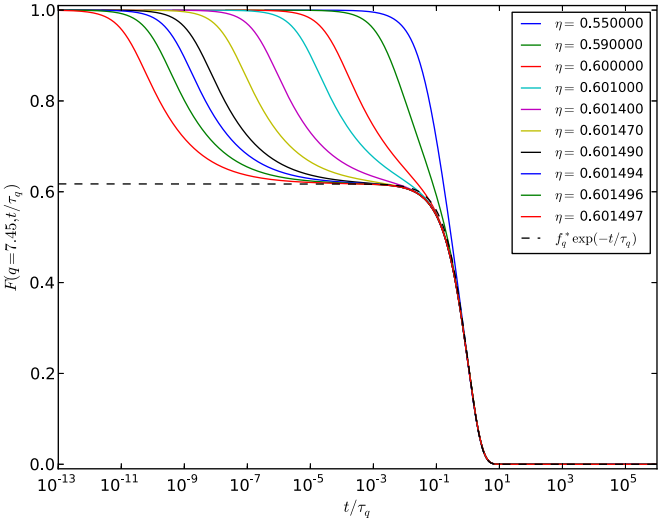

FIG. 5. (Color online) The intermediate structure factor is plotted for several densities against scaled time t/τ_q, where τ_q is found as the effective time constant of the stretched exponential, Eq. (56); values of packing fraction increase from curve to curve with the the rightmost solid curve being the lowest value ($\eta = 0.550000$) and the leftmost solid curve being the highest value ($\eta = 0.601497$). As τ_q is proportional to τ_α, the long-time behavior—from the von Schweidler decay out of the plateau through the α relaxation to zero—collapses onto one curve under such a transformation. We plot an exponential function of the form $f_q \exp(-t/\tau_q)$ (dotted curve) for comparison showing that the α relaxation is well approximated by a stretched exponential with β very close to 1.

the easiest to extract. Rewriting Eq. (55) here, we have

$$\tau_q = \frac{\theta_0}{|\epsilon|^\gamma} = \frac{\theta_0 \eta^*}{(\eta^* - \eta)^\gamma}, \tag{59}$$

where again $\gamma = 1/2a + 1/2b$ and where θ_0 is a fitting parameter proportional to the microscopic time scale, τ_0.

Fitting several α-relaxation decays at different densities, we extract τ_q and plot the collapsed function $F(q,t/\tau_q)$ in Fig. 5; all curves collapse to one from the von Schweidler decay through the stretched exponential decay to zero. We show the explicit scaling of τ_q as a function of density for select values of wave number in Fig. 6. Power-law fits to this data find $\gamma = 1.887(4)$ where the uncertainty is given by the small spread in fit values at different wave numbers.

If we combine the equation $\gamma = 1/2a + 1/2b$ with the constraint given by λ, Eq. (54), we identify a unique set of exponents and find

$$a = 0.375(3), \quad b = 0.887(4), \quad \lambda = 0.5587(18). \tag{60}$$

3. *Verifying the predicted exponents for the intermediate structure factor, F(q,t)*

In the ergodic phase, we fit to the form

$$F(q,t) = \begin{cases} f_a + h_q(t/\tau_0)^{-a} & : \tau_0 \ll t \ll \tau_\beta \\ f_b - h_q(t/\tau_\alpha)^b & : \tau_\beta \ll t \ll \tau_\alpha \end{cases}, \tag{61}$$

where we fix a, b, and h_q but allow the other parameters to vary. Note that we have allowed the plateau value—f_a in the first line and f_b in the second—to be fit independently at the early and late times even though we expect the value to be the same in both fits; this constraint is recovered naturally when the appropriate domain for the fit is selected.

In the nonergodic phase, we fit to

$$F(q,t) = f_a + h_q(t/\tau_0)^{-a} \ : \tau_0 \ll t \ll \tau_\beta, \tag{62}$$

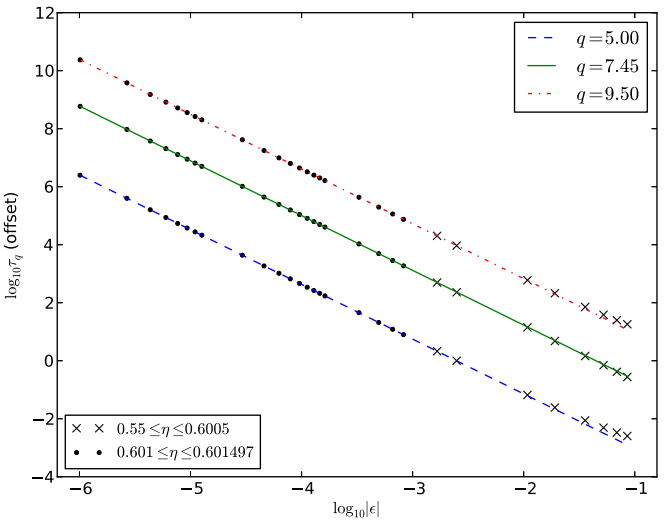

FIG. 6. (Color online) Fits of the time scale τ_q to Eq. (IIIC2) for select values of wave number are shown on a log-log scale such that each curve is linear with slope $\gamma = 1/2a + 1/2b = 1.887$. Only points for $\eta \geq 0.601$ ($|\epsilon| \leq 10^{-3}$) were used in the fit, though the fit function is extended down to $\eta = 0.55$ to show where the data depart from the model. (Note that the curve and data for $q = 9.50$ has been artificially shifted up by two units and $q = 5.00$ shifted down by two units in order to prevent data sets from overlapping on the plot. Scaling is unaffected.)

where again we keep h_q and a fixed and expect f_a to approach the critical nonergodicity factor as the fit domain choice improves.

As discussed above, picking domain cuts by eye can lead to great variation, but we institute a set of criteria to determine the optimal domain:

(i) First, it is expected that the system will decay into and out of a plateau value which is equal to the critical value of the nonergodicity factor. Therefore, the optimal domain will yield $f_a \approx f_b \approx f_q^*$.

(ii) Second, for the early part of the β-relaxation decay, note that τ_0 is a constant independent of both wave number and density. Therefore, the optimal domain over this part of the data can be found and set once; it will yield identical results as we change wave number and as we change density (provided we remain close to the transition where ϵ is small).

(iii) Third, the time scale τ_α depends on density but not on wave number. The optimal domain over the late part of the β regime will yield consistent values for τ_α as we vary q.

(iv) Finally, the optimal time scale will show the smallest residual between data and fit. Visually, we will verify this by plotting $\log_{10}(|F(q,t) - f_q^*|)$ versus $\log_{10} t$, where the fit is expected to be a straight line and where deviations from the data will be most clear.

In Figs. 7 and 8, we show our the results on either side of the transition for $\eta = 0.601497$ and $\eta = 0.601498$ at $q = 7.45$ near the static structure factor maximum. As can be seen visually, each domain is only a few decades long, but the data match the model well and the exponent values capture the decays appropriately.

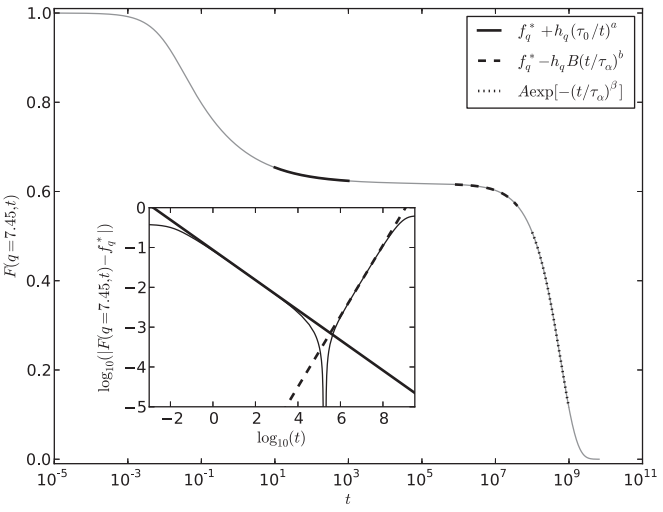

FIG. 7. Values of a and b were found as the solution to the set of coupled equations for λ and γ where the value of γ was found by the fit of τ_q as a function of density. These values were used along with the value of h_q found from the nonergodicity factor fit as fixed parameters in fits to the early and late portions of the β relaxation of $F(q,t)$. Shown here are the two power-law fits (into and out of the plateau) as well as the stretched exponential fit of the late time α regime for $\eta = 0.601497$ just below the transition and $q = 7.45$ near the first structure factor maximum. The inset shows the power-law fits plotted on a log-log scale. Several decades of data lie along the fit functions showing good agreement with the model.

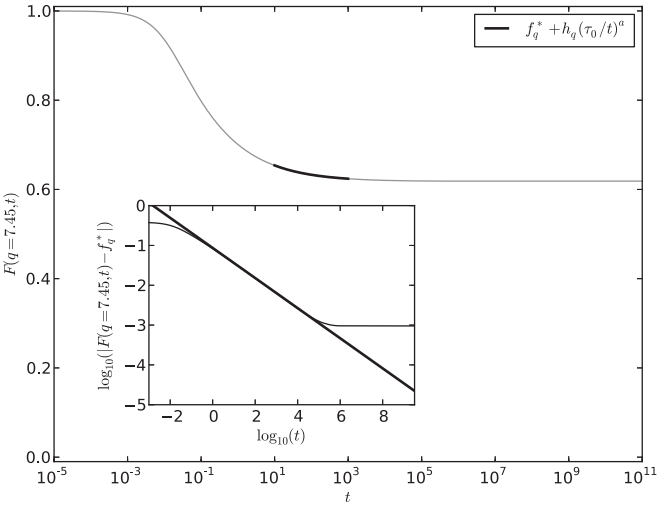

FIG. 8. Values of a and b were found as the solution to the set of coupled equations for λ and γ where the value of γ was found by the fit of τ_q as a function of density. These values were used along with the value of h_q found from the nonergodicity factor fit as fixed parameters in fits to the early and late portions of the β regime of $F(q,t)$. Shown here is the single power-law fit for $\eta = 0.601498$ just above the transition at $q = 7.45$. The inset shows the power-law fit plotted on a log-log scale. We see that several decades of data lie along the fit function showing good agreement with the model.

4. Direct fit to the intermediate structure factor, F(q,t)

While the above verification worked well, it it valid to ask if the exponent values (and other fit values) could be found directly from the β-regime data. As cautioned in the introduction to this section, this is less straightforward than expected due to the variability caused by domain choice, but we will show here that the results are consistent with what we found above.

Again, let us perform a constrained fit on the function $F(q,t)$ in the ergodic phase using Eqs. (61) and (62), but this time allowing a and b to vary. (The critical amplitude h_q remains fixed.) The best fit values are those which minimize the squares of the residuals, satisfy the exponent constraint, Eq. (54), and converge to $f_a \approx f_b \approx f_b$.

Doing this fit for values of density just below the transition, we find robust values for the exponents

$$a = 0.374(10), \quad b = 0.878(8), \quad \lambda = 0.568(16). \tag{63}$$

Uncertainties here again represent a small spread in values from fits at different wave number and density and are slightly larger than in the previous method. The results, however, are consistent and we see that a suitable and reliable method is possible despite the difficulties of the fit.

IV. COMPARISON TO OTHER WORK

Let us very briefly mention other theoretical, experimental and numerical work on hard-sphere transitions. Such a discussion cannot be exhaustive, but can give our results some context. We compile a limited number of numerical values for comparison in Table I and refer the reader to reviews such as Refs. [37,38,67] for more information.

TABLE I. This table compares the transition density and exponents for select hard-sphere (colloidal) theories, experiments, and simulations. For replica theory, the dynamic transition density η_d can be compared to MCT-like transition densities η^*, while the static transition density η_K can be compared to ideal glass transition densities η_0. For both the experiments and simulations listed, only values of the exponent γ are reported by the authors; values for λ, a, and b are inferred as described in the text. Transitions labeled "power-law divergence" correspond to fitting τ_α to the MCT divergence of Eq. (55), while transitions labeled "exponential divergence" correspond to fitting τ_α to the Vogel-Fulcher-Tammann form of Eq. (64) which models activated dynamics.

Theory, experiment, or simulation	Critical density	Exponents
Mazenko theory (Percus-Yevick)	$\eta^* = 0.60149761(10)$	$a = 0.375(3)$, $b = 0.887(4)$, $\gamma = 1.887(4)$, $\lambda = 0.5587(18)$
Mode-coupling theory [35,68] (Percus-Yevick)	$\eta^* = 0.515(10)$	$a = 0.312$, $b = 0.584$, $\gamma = 2.5$, $\lambda = 0.734$
Replica theory [37] (hypernetted chain)	$\eta_d = 0.619$ $\eta_K = 0.63$	–
(first-order small cage expansion)	$\eta_K = 0.6175$	–
Colloidal experiment [36] (power-law divergence)	$\eta^* = 0.590(5)$	$a = 0.308(10)$, $b = 0.57(3)$, $\gamma = 2.5(1)$, $\lambda = 0.743(20)$
(exponential divergence)	$\eta_0 = 0.637(2)$	$\delta = 2.0(2)$
Monte Carlo simulation [36,69] (power-law divergence)	$\eta^* = 0.590(5)$	$a = 0.308(10)$, $b = 0.57(3)$, $\gamma = 2.5(1)$, $\lambda = 0.743(20)$
(exponential divergence)	$\eta_0 = 0.651(2)$	$\delta = 2.0(2)$
Langevin dynamics simulation [38] (power-law divergence)	$\eta^* = 0.595(1)$	$a = 0.314$, $b = 0.583$, $\gamma = 2.445$, $\lambda = 0.735$

A. Mode-coupling theory

As said in the Introduction, mode-coupling theory is an *incomplete* theory of the glass transition. Nearly since its introduction, users have noted its limitations, including that while certain experiments and simulations are well modeled by the *form* of the MCT equations, some of the parameters predicted by the theory—such as the transition density (or temperature)—do not agree with real data.

In recent years, it has been established that MCT is a Landau (mean-field) theory [22,70] which helps to explain why the above-mentioned features are in fact universal. This places MCT on firmer ground and sheds light on why we find (and in fact should expect) that the theory described in this paper follows many of the same functional forms [35].

Mode-coupling theory predicts a transition at $\eta^* = 0.505(10)$ [68] with critical exponents $\lambda = 0.734$, $a = 0.312$, $b = 0.584$, and $\gamma = 2.5$ [35]. This transition density is well below what we find in this work, but it is low compared to all other theories and numerical data as well. Our exponent values also differ somewhat from MCT's, even though the relationships between them hold.

The nonergodicity factor f_q and critical amplitude h_q which we derive in this paper show qualitative similarity to MCT (see Figs. 2 and 4) but differ in quantitative ways; our results are more narrowly peaked around the wave numbers of the structure factor maxima than MCT's and have different amplitudes, and we have significantly less weight in both functions at low wave number between $q = 0$ and the first peak. Measurements of f_q and h_q from numerical and experimental work on hard spheres soon after the debut of MCT match the MCT forms more closely than our forms (see, e.g., Fig. 3 in Ref. [25]) as does more recent simulation work (see, e.g., Figs. 5 and 10 in Ref. [38]).

B. Other theories

Initial efforts to "derive" MCT using kinetic theory were only crudely successful. In order to gain some control, effective dynamical field theories were introduced, beginning with the realization that MCT can be understood in terms of the fluctuating nonlinear hydrodynamics of dense fluids [71–73]. In this approach, however, the formal structure of the field theory is sufficiently complex that it is difficult to go beyond one-loop order in the calculation. Next came the Dean-Kawasaki model [74–78], the simplest field-theoretic model that describes the kinetics of the colloidal systems operating under Smoluchowski dynamics. Initially, this theory also ran aground, though recent efforts have overcome these difficulties and show the model does not support an ergodic-nonergodic transition at one-loop order [79]. Further numerical work is needed before more careful comparisons can be made.

Other, more complicated, field-theoretic models have been put forth [80–87]. The use of effective field theories turns out to be technically as complicated as a microscopic approach with the drawback of not reproducing the correct statics and the need to introduce a large wave-number cutoff. At least one theory has derived "correction" terms to MCT which indicate a push to higher transition density for hard spheres [88]; however, again, complications keep the discussion to qualitative statements only.

One recent popular approach is to explore the glass transition through the lens of random first-order transition (RFOT) theory [89] and the related replica theory [37,90,91]. We cannot discuss details here, but, importantly, the theory is able to produce *quantitative* results using equilibrium dynamics information such as $S(q)$ as input—just as MCT and the theory of this paper.

Replica theory does not predict an ergodic-nonergodic transition *per se* but instead identifies two transition densities.

The lower of the two, the dynamic transition η_d, is the density at which glassy states first appear; this can be associated at the mean-field level with a MCT-like transition. The higher of the two, the static transition η_K, is the "ideal" or "thermodynamic glass transition" where there is a jump in the compressibility; this transition can be associated with the divergence of the equilibrium relaxation time or with the Kauzmann transition.

Replica theory applied to hard spheres with the hypernetted chain (HNC) closure scheme predicts values of $\eta_d = 0.619$ and $\eta_K = 0.63$ [37,92,93], both of which are larger than η^* found for MCT and the theory presented here. The theory also produces a nonergodicity factor f_q (see Ref. [37], Fig. 10) which shares some qualitative features with that of MCT at the critical density but which quantitatively differs in significant ways; the peaks are located at the wave numbers of the structure factor maxima but are narrower than in MCT (like our results in this paper) and have a lower amplitude overall. There also is much less weight at $q = 0$ (again, like our result.)

The HNC closure, however, leads to some other nonphysical results in replica theory, and for that reason, a new approach has been explored. Using what is called the "first-order small cage approximation," a more robust derivation yields an estimate of $\eta_K = 0.6175$ [37]. Unfortunately, under this approximation no correlation functions or nonergodicity factors can be computed.

C. Experiment and simulation

If one wishes to compare our work here on hard spheres obeying Smoluchowski dynamics to experiment, the closest realization is a colloidal suspension where particles interact only through repulsion on contact—a hard-sphere potential, to good approximation [62].

Beginning soon after after mode-coupling theory was developed, many colloidal experiments have been performed to check the validity of the theory [14,15,94–96]. This work established that the MCT prediction for the glass-transition density of $\eta^* = 0.505(1)$ is too low, though measurements of the actual transition density have been in conflict; typical values span a range $0.57 \leqslant \eta^* \leqslant 0.60$, up against the limit of what can be made and measured in the laboratory. Results, however, do lend credence to the predicted power-law forms describing the relaxation, and the MCT exponents plausibly match these experiments given the limits of power-law fits to sparse data [25].

Advances in recent years, however, have allowed for both more sophisticated experiments and simulations. Let us look at a few of these studies in particular.

First, in the most complete colloidal study to date, dynamic light scattering is used to measure concentrations of colloidal hard spheres up to a density of $\eta = 0.5970$ [36]. Though the system remains ergodic over the entire range studied, there is tremendous slowing down and over seven decades of relaxation time, τ_α. The authors find that a fit of these relaxation times for $0.49 < \eta \leqslant 0.585$ yields a power-law divergence [Eq. (55)] at critical density $\eta^* = 0.590(5)$ with power-law exponent $\gamma = 2.5(1)$.

This result, however, contradicts the experiment; the system clearly remains ergodic above this critical density. To resolve this, the authors find that when including data for $\eta > 0.585$, the divergence is better modeled as an exponent of the Vogel-Fulcher-Tammann form [97–99]

$$\tau_\alpha(\eta) = \tau_\infty \exp\left[\frac{A}{(\eta_0 - \eta)^\delta}\right] \tag{64}$$

with $\delta = 2.0(2)$ and $\eta_0 = 0.637(2)$. The authors interpret the avoidance of the power-law-type divergence as evidence of a crossover to an "activated" regime where hopping modes not addressed by MCT (or our theory) become important. This interpretation is debated [100] and it is unclear if such hopping processes should even be accessible in a hard sphere or colloidal system [105]. This work, however, remains the only data set with sufficient resolution at such high densities to allow comparison between the two divergence forms at all.

In the same work and a related study [69], the authors also ran Monte Carlo hard-sphere simulations. Power-law divergence fits to the same density ranges above yielded an identical critical density $\eta^* = 0.590(5)$ and critical exponent $\gamma = 2.5(1)$. Fitting to the alternate exponential-divergence yielded an even higher divergence density $\eta_0 = 0.651(2)$ than the experiment.

Though both the experimental and simulation work covers a wide time range, the authors make no attempt to fit power-law functions to the decays into and out of the plateau of the β regime in either the experimental or simulation case. However, coupling the authors' value for γ with the λ constraint (just as we do for our own work here), the predicted exponents are $a = 0.308(10)$ and $b = 0.57(3)$, with $\lambda = 0.743(20)$. These are consistent with the prediction of MCT using Percus-Yevick hard spheres quoted above but differ from the values we find in our own solution.

A second, different, computational study that should be mentioned is a recent strongly damped molecular-dynamics (Langevin dynamics) simulation of polydisperse hard spheres up to a packing fraction of $\phi = 0.585$ [38]. This work, in particular, studied differences between collective and tagged-particle density-density correlation functions and performed a rigorous comparison to MCT predictions. As discussed above in Sec. IV A, the forms of f_q^* and h_q quantitatively match MCT well and the scaling laws of the dynamic results were tested and verified. Though the simulation does not go to high-enough density to observe an ergodic-nonergodic transition, fitting the power-law divergence of the time scale yields a transition density of $\eta^* = 0.595(1)$, consistent with the simulations and experiments discussed previously. The authors, however, observe no evidence of a crossover to activated dynamics.

V. CONCLUSION

We have reviewed a theory which derives the governing kinetic and static equations for n-point cumulant functions between density and response fields for systems of particles obeying either Newtonian or Smoluchowski dynamics in a self-consistent perturbation expansion in the effective interparticle potential. At second order, we find that the density-density cumulant obeys a kinetic equation similar to that seen in mode-coupling theory with a memory function quadratic in the potential and quadratic in the cumulant itself. In the long-time limit, this equation supports an ergodic-nonergodic transition and we outline an asymptotic analysis (the same as mode-coupling theory's) that predicts a two-step decay

with associated diverging time scales, and power-law decays into and out of an extended plateau with wave-number- and density-independent exponents.

For a simple model system of hard spheres obeying Smoluchowski dynamics, we solve for the full behavior of the intermediate structure factor at all wave numbers and over a wide range of densities from dilute fluid to maximally dense. Near the transition, the intermediate structure factor evolves from an exponential decay into the two-step decay characteristic of supercooled liquids, and the relaxation slows by orders of magnitude. At even higher density, we pass the critical packing fraction and the correlation function decays only to a finite plateau, showing that the system has naturally selected the nonergodic solution. This work represents the first numerical solution showing the full dynamics near an ergodic-nonergodic transition outside of mode-coupling theory and covers an unprecedented nearly 15 decades of scaled time. The long-time results of the full dynamics match earlier studies of the statics under the same theory and we recover the previously investigated nonergodicity factors and critical transition density $\eta^* = 0.60149761(10)$.

As part of this solution, we test the results using two forms for the memory function at second order in the potential. The first is the so-called long-time form where we drop the self-contribution and simplify the collective contribution. The second is a a more complete form which keeps all terms but uses the zeroth-order approximation for the vertex functions. In this latter solution, we again monitor the density-density time correlation function $F(q,t)$ but also compute two dressed propagators, $\bar{F}(q,t)$ and $\tilde{F}(q,t)$, which modify short-time behavior but not the long-time limit. We find that the two solutions behave exactly as expected and that the universal features of the approach to the ergodic-nonergodic transition are identical in both cases. In fact, the two solutions can be mapped onto each other with a simple scaling of the microscopic time $\tau_0 \to \tau_0'$ in all the appropriate equations. This equivalence justifies *a posteriori* the assumptions implicit in the asymptotic expansion approximation and reinforces the similarities seen between the MCT memory function and the long-time approximate memory function derived here.

Using the full dynamic solution, we were able to investigate the two time scales which are relevant in the ergodic regime—τ_α, which sets the time scale of the long-time relaxation to zero, and τ_β, which sets the scale of the time spent in the intermediate plateau. Both time scales are seen to diverge as the density increases to the critical density and from the power-law scaling of τ_α, we extract our first critical exponent, $\gamma = 1.887(4)$. This exponent is in turn related to the other two exponents as $\gamma = 1/2a + 1/2b$. In conjunction with the critical exponent parameter,

$$\lambda = \frac{\Gamma^2(1-a)}{\Gamma(1-2a)} = \frac{\Gamma^2(1+b)}{\Gamma(1+2b)}, \tag{65}$$

we found $a = 0.375(3)$, $b = 0.887(4)$, and $\lambda = 0.5587(18)$. These are consistent with parameters extracted from direct fits to $F(q,t)$ where $a = 0.374(10)$, $b = 0.878(8)$, and $\lambda = 0.568(16)$.

In functional form, our solution matches the most important features seen in experiment and simulation and predicted by mode-coupling theory. The transition density we find at this order is similar to the range of values seen in polydisperse colloidal suspensions, hard-sphere simulations, and replica theory, but our universal exponents do differ from these and from MCT. Additionally, our nonergodicity factor f_q and critical amplitude h_q share qualitative features with measured or predicted forms but do not match quantitatively. Crucially, however, this need not be the end of the story. Unlike MCT, this theory has a clear method for calculating corrections and we are in a position to explore how the physics evolve order by order. Understanding how the values of these universal exponents and form factors change as we include higher-order terms will be an interesting future undertaking.

The numerical solution here establishes this new theory as a viable alternative to mode-coupling theory and one derived from first principles with a self-consistent expansion that is well motivated on physical grounds. Many salient features of the glass transition emerge naturally and we see that the results can be analyzed with the same critical dynamics machinery pioneered in MCT.

The first parameter estimates here are tantalizing, but a host of new tests await. This theory can be extended to study multicomponent systems or systems trapped in external fields [111,112], to look at four-point correlation functions and investigate the growing length scales thought to be associated with dynamic heterogeneity [55–59], to study systems in dimension higher than $d = 3$ and to compare with other theories in large dimension limits [37,70], or to further investigate the equivalence between the long-time limits of Newtonian and Smoluchowski dynamics [33,40].

ACKNOWLEDGMENTS

The author extends his sincerest thanks to Professor Gene Mazenko for his guidance and direction on this work and for guiding him through many years as a student. The author also thanks Paul Spyridis for many helpful conversations and specifically acknowledges Mr. Spyridis's help bringing to his attention the numerical algorithms used here for solving the kinetic equation quickly and efficiently. Thanks also to P. Spyridis for providing the MCT data used in Figs. 2 and 4. This work was supported by the Department of Physics at the University of Chicago and by the United States Department of Education under Graduate Assistance in Areas of National Need (GAANN).

APPENDIX: THE DRESSED PROPAGATORS AND THE NO-VERTEX APPROXIMATION SOLUTION

The dressed propagators naturally appear in the theory as one computes the kinetic equation at second or higher order. The two cumulants which appear in this work are given in the frequency domain by

$$\bar{G}_{\alpha\beta}(12) = \frac{1}{2}\big[G^{(0)}_{\alpha\gamma}(13)\sigma_{\gamma\delta}(34)G_{\delta\beta}(42) + G_{\alpha\gamma}(13)\sigma_{\gamma\delta}(34)G^{(0)}_{\delta\beta}(42)\big] \tag{A1}$$

and

$$\tilde{G}_{\alpha\beta}(12) = G^{(0)}_{\alpha\gamma}(13)\sigma_{\gamma\delta}(34)G_{\delta\epsilon}(45)\sigma_{\epsilon\zeta}(56)G^{(0)}_{\zeta\beta}(62). \tag{A2}$$

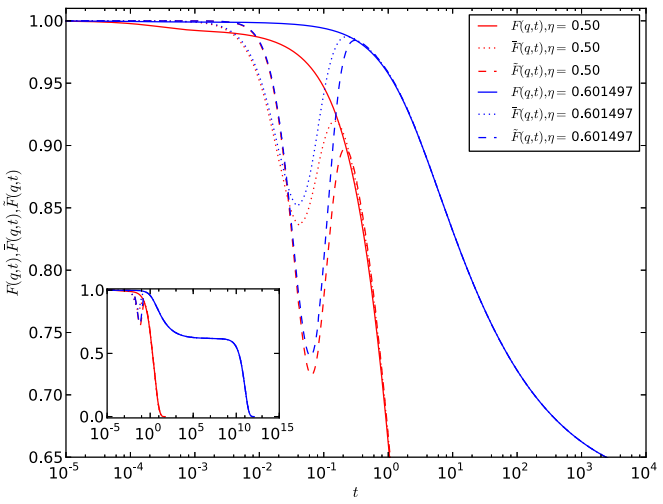

FIG. 9. (Color online) The dressed propagators $\bar{F}(q,t)$ and $\tilde{F}(q,t)$ are shown alongside the full intermediate static structure factor $F(q,t)$ at wave number $q = 7.45$ and at two densities. The family of curves to the left which decays quickly to zero corresponds to $\eta = 0.5$, well below the transition. The family of curves to the right which shows the intermediate time plateau corresponds to $\eta = 0.601497$, very close to the transition. The full functions are plotted in the inset, but the main plot shows just the short-time portion where the three propagator functions differ. Note that the dressed propagators decay quickly but then change sign and actually increase to meet $F(q,t)$. Despite the very different long-time behaviors, the dressed propagators at these two packing fractions both "dip" to roughly the same values at roughly the same times, meaning that this anomalous behavior is not highly dependent on density.

Moving to the time domain, the normalized $\rho\rho$ components become

$$\bar{F}(q,t) = F^{(0)}(q,t) + q^2 \int_0^t ds F^{(0)}(q,t-s)F(q,s) \quad \text{(A3)}$$

and

$$\tilde{F}(q,t) = F^{(0)}(q,t)[1+q^2|t|] + q^4 \int_0^t ds|t-s|F^{(0)}(q,t-s)F(q,s). \quad \text{(A4)}$$

Solving the kinetic equation using the full second-order memory function without vertex corrections, Eq. (40) shows us that $\bar{F}(q,t)$ and $\tilde{F}(q,t)$ behave as predicted—they decay quicker than $F(q,t)$ at short times but approach $F(q,t)$ at long times. Plots of all three correlations functions are given in Fig. 9.

Furthermore, the solution for the full function $F(q,t)$ is identical to that found with the long-time approximate form for the memory function, Eq. (48), with a rescaling of the microscopic time $\tau_0 \to \tau_0'$. Both solutions show the same two-step decay with identical exponents, and the time scales τ_α and τ_β show the same power-law divergences. The nonergodicity factors and the critical density at which the ergodic-nonergodic transition occurs are likewise identical.

For completeness, we include here the discretizations and approximations used to compute the dressed propagators and solve the kinetic equation for the no-vertex corrections memory function form. This discretization is analogous to that used for the full propagator and memory function of Fuchs *et al.* [64,65] used elsewhere in this work.

The first dressed propagator is given by

$$\bar{F}(q,t) = F^{(0)}(q,t) + q^2 \int_0^t ds F(q,s)F^{(0)}(q,t-s), \quad \text{(A5)}$$

which can be split and integrated by parts to give

$$\bar{F}(q,t) = F^{(0)}(q,t) - F^{(0)}(q,t-t/2)F(q,t/2) + F^{(0)}(q,0)F(q,t) + q^2 \int_0^{t/2} ds F(q,s)F^{(0)}(q,t-s) + \int_0^{t-t/2} ds F^{(0)}(q,s)\frac{\partial}{\partial s}F(q,t-s). \quad \text{(A6)}$$

The first integral can be approximated as

$$q^2 \int_0^{t/2} ds F(q,s)F^{(0)}(q,t-s) \approx q^2 F^{(0)}(q,t) \sum_{m=1}^{j/2} \int_{t_{m-1}}^{t_m} ds F(q,s)e^{q^2 s}, \quad \text{(A7)}$$

and, if we define

$$d\bar{F}(q_i,t_m) \equiv \frac{1}{\Delta_t}\int_{t_{m-1}}^{t_m} ds F(q_i,s)e^{q_i^2 s} \approx \frac{e^{q_i^2 t_m}F(q_i,t_m) + e^{q_i^2 t_{m-1}}F(q_i,t_{m-1})}{2}, \quad \text{(A8)}$$

where Δ_t is the time step, we then have

$$q^2 \int_0^{t/2} ds F(q,s)F^{(0)}(q,t-s) \approx q^2 \Delta_t F^{(0)}(q,t) \sum_{m=1}^{j/2} d\bar{F}(q,t_m). \quad \text{(A9)}$$

The second integral similarly becomes

$$\int_0^{t-t/2} ds F^{(0)}(q,s)\frac{\partial}{\partial s}F(q,t-s) \approx \sum_{m=1}^{j-j/2}\left[\frac{F(q,t-t_m)-F(q,t-t_{m-1})}{\Delta_t}\right]\left(\frac{-1}{q^2}\right)[e^{-q^2 t_m} - e^{-q^2 t_{m-1}}]. \quad \text{(A10)}$$

Plugging these terms back into Eq. (A5) and introducing a discrete notation $g(q,t) \rightarrow g[i][j]$ and wave-number step Δ_q, we compactly write

$$\bar{F}[i][j] = C[i]F[i][j] + D[i][j], \tag{A11}$$

where

$$C[i] = \frac{F^{(0)}[i][0][(i\Delta_t)^2\Delta_t - 1] + F^{(0)}[i][1]}{(i\Delta_q)^2\Delta_t} \tag{A12}$$

and

$$D[i][j] = F^{(0)}[i][j]\left[1 + (i\Delta_q)^2\Delta_t \sum_{m=1}^{j/2} d\bar{F}[i][m]\right] - F^{(0)}[i][j - j/2]F[i][j/2] + \left(\frac{1}{(i\Delta_q)^2\Delta_t}\right) \sum_{m=2}^{j-j/2}$$
$$\times [F[i][j-m] - F[i][j-m-1]][F^{(0)}[i][m-1] - F^{(0)}[i][m]] + F[i][j-1]\left[\frac{F^{(0)}[i][0] - F^{(0)}[i][1]}{(i\Delta_q)^2\Delta_t}\right]. \tag{A13}$$

At $q = 0$, these reduce to $C[0] = 1$ and $D[0] = 0$, yielding $\bar{F}[0][j] = 1$ as expected.

The second dressed propagator is given by

$$\tilde{F}(q,t) = F^{(0)}(q,t)[1 + q^2 t] + q^4 \int_0^t ds(t-s)F(q,s)F^{(0)}(q,t-s). \tag{A14}$$

Defining

$$d\tilde{F}(q_i,t_m) \equiv \frac{1}{\Delta_t}\int_{t_{m-1}}^{t_m} ds s F(q_i,s)e^{q_i^2 s} \approx \frac{t_m e^{q_i^2 t_m} F(q_i,t_m) + t_{m-1}e^{q_i^2 t_{m-1}} F(q_i,t_{m-1})}{2}, \tag{A15}$$

we can follow the same logic as above and write this compactly as

$$\tilde{F}[i][j] = E[i]F[i][j] + Z[i][j], \tag{A16}$$

where

$$E[i] = 1 + F^{(0)}[i][[1] \tag{A17}$$

and

$$Z[i][j] = F^{(0)}[i][j]\left[1 + (i\Delta_q)^2 t + (i\Delta_q)^4\Delta_t \sum_{m=1}^{j/2}(j\Delta_t d\bar{F}[i][m] - d\tilde{F}[i][m])\right]$$
$$- F^{(0)}[i][j - j/2]F[i][j/2][1 + (i\Delta_q)^2(j - j/2)\Delta_q] - F[i][j-1]F^{(0)}[i][1]$$
$$+ \left(\frac{1}{(i\Delta_q)^2\Delta_t}\right)\sum_{m=2}^{j-j/2}[F[i][j-m] - F[i][j-m-1]]$$
$$\times \left[(2 + (i\Delta_q)^2(m-1)\Delta_t)e^{-(i\Delta_q)^2(m-1)\Delta_t} - (2 + (i\Delta_q)^2 j\Delta_t)e^{-(i\Delta_q)^2 m\Delta_t}\right]. \tag{A18}$$

At $q = 0$, these reduce to $E[0] = 2$ and $Z[0][j] = -1$, yielding $\tilde{F}[0][j] = 1$, as expected.

Just as the intermediate structure factor and memory function are updated as the step size is doubled, the dressed propagator arrays will also need to be updated. This is accomplished as follows:

$$\bar{F}[i][j] \rightarrow \bar{F}[i][2j], \tag{A19}$$

$$\tilde{F}[i][j] \rightarrow \tilde{F}[i][2j], \tag{A20}$$

$$d\bar{F}[i][j] \rightarrow \left(e^{-(i\Delta_q)^2(2j)\Delta_t}F[i][2j] + 4e^{-(i\Delta_q)^2(2j-1)\Delta_t}F[i][2j-1] + e^{-(i\Delta_q)^2(2j-2)\Delta_t}F[i][2j-2]\right)/6, \tag{A21}$$

$$d\tilde{F}[i][j] \rightarrow \left((2j)\Delta_t e^{-(i\Delta_q)^2(2j)\Delta_t}F[i][2j] + 4(2j-1)\Delta_t e^{-(i\Delta_q)^2(2j-1)\Delta_t}F[i][2j-1] + (2j-2)\Delta_t e^{-(i\Delta_q)^2(2j-2)\Delta_t}F[i][2j-2]\right)/6. \tag{A22}$$

[1] F. H. Stillinger, Science **267**, 1935 (1995).

[2] M. D. Ediger, C. A. Angell, and S. R. Nagel, J. Phys. Chem. **100**, 13200 (1996).

[3] C. A. Angell, K. L. Ngai, G. B. McKenna, P. F. McMillan, and S. W. Martin, J. Appl. Phys. **88**, 3113 (2000).

[4] W. Götze and L. Sjögren, Rep. Prog. Phys. **55**, 241 (1992).

[5] P. K. Dixon, L. Wu, S. R. Nagel, B. D. Williams, and J. P. Carini, Phys. Rev. Lett. **65**, 1108 (1990).

[6] L. Börjesson, M. Elmroth, and L. M. Torell, Chem. Phys. **149**, 209 (1990).

[7] W. Petry, E. Bartsch, F. Furuja, M. Kiebel, H. Sillescu, and B. Farago, Z. Phys. B **83**, 175 (1991).

[8] G. Li, W. M. Du, X. K. Chen, H. Z. Cummins, and N. J. Tao, Phys. Rev. A **45**, 3867 (1992).

[9] G. Li, W. M. Du, A. Sakai, and H. Z. Cummins, Phys. Rev. A **46**, 3343 (1992).

[10] D. L. Sidebottom, R. Bergman, L. Börjesson, and L. M. Torrell, Phys. Rev. Lett. **68**, 3587 (1992).

[11] I. C. Halalay and K. A. Nelson, Phys. Rev. Lett. **69**, 636 (1992).

[12] P. G. Debenedetti and F. H. Stillinger, Nature (London) **410**, 259 (2001).

[13] S.-H. Chong and M. Fuchs, Phys. Rev. Lett. **88**, 185702 (2002).

[14] P. N. Pusey and W. van Megen, Phys. Rev. Lett. **59**, 2083 (1987).

[15] W. van Megen, T. C. Mortensen, S. R. Williams, and J. Müller, Phys. Rev. E **58**, 6073 (1998).

[16] Z. Cheng, J. Zhu, P. M. Chaikin, S.-E. Phan, and W. B. Russel, Phys. Rev. E **65**, 041405 (2002).

[17] S.-E. Phan, W. B. Russel, Z. Cheng, J. Zhu, P. M. Chaikin, J. H. Dunsmuir, and R. H. Ottewill, Phys. Rev. E **54**, 6633 (1996).

[18] E. Leutheusser, Phys. Rev. A **29**, 2765 (1984).

[19] W. Götze, Z. Phys. B **56**, 139 (1984).

[20] U. Bengtzelius, W. Götze, and A. Sjölander, J. Phys. C **17**, 5915 (1984).

[21] W. Götze, Z. Phys. B **60**, 195 (1985).

[22] A. Andreanov, Glass transition: A mean-field theory, Ph.D. thesis, École Polytechnique, 2007.

[23] W. Götze, J. Phys.: Condens. Matter **2**, SA201 (1990).

[24] W. Götze, in *Liquids, Freezing and Glass Transition*, edited by J.-P. Hansen, D. Levesque, and J. Zinn-Justin (North-Holland, Amsterdam, 1991), p. 287.

[25] W. Götze, J. Phys.: Condens. Matter **11**, A1 (1999).

[26] S. P. Das, Rev. Mod. Phys. **76**, 785 (2004).

[27] W. Götze, *Complex Dynamics of Glass-Forming Liquids: A Mode-Coupling Theory* (Oxford University Press, New York, 2009).

[28] D. R. Reichman and P. Charbonneau, J. Stat. Mech. (2005) P05013.

[29] G. F. Mazenko, Phys. Rev. E **81**, 061102 (2010).

[30] G. F. Mazenko, Phys. Rev. E **83**, 041125 (2011).

[31] S. P. Das and G. F. Mazenko, J. Stat. Mech. **149**, 643 (2012).

[32] S. P. Das and G. F. Mazenko, J. Stat. Phys. **152**, 159 (2013).

[33] G. F. Mazenko, Phys. Rev. E **89**, 022110 (2014).

[34] G. F. Mazenko, D. D. McCowan, and P. Spyridis, Phys. Rev. E **85**, 051105 (2012).

[35] P. Spyridis and G. F. Mazenko, J. Stat. Phys. **154**, 1030 (2014).

[36] G. Brambilla, D. El Masri, M. Pierno, L. Berthier, L. Cipelletti, G. Petekidis, and A. B. Schofield, Phys. Rev. Lett. **102**, 085703 (2009).

[37] G. Parisi and F. Zamponi, Rev. Mod. Phys. **82**, 789 (2010).

[38] F. Weysser, A. M. Puertas, M. Fuchs, and T. Voigtmann, Phys. Rev. E **82**, 011504 (2010).

[39] As shown in Ref. [33], the theory predicts that the short-time dynamics of these two types of systems will differ substantially (ballistic versus Brownian) but converge to the same long-time dynamics. This is consistent with simulations [40–42]. Importantly for our development here, the differences between the two dynamics types can all be rolled into the definition of the response field and the calculation of the zeroth-order cumulants and vertices; the remaining formalism is identical.

[40] G. Szamel and E. Flenner, Europhys. Lett. **67**, 779 (2004).

[41] T. Gleim, W. Kob, and K. Binder, Phys. Rev. Lett. **81**, 4404 (1998).

[42] F. Höfling, T. Munk, E. Frey, and T. Franosch, J. Chem. Phys. **128**, 164517 (2008).

[43] P. C. Martin, E. D. Siggia, and H. A. Rose, Phys. Rev. A **8**, 423 (1973).

[44] R. Bausch, H. J. Janssen, and H. Wagner, Z. Phys. B **24**, 113 (1976).

[45] While these two fields cover essentially all the degrees of freedom of interest in a Smoluchowski system, the momentum degrees of freedom of a Newtonian system lead to additional conservation laws and one may want to look in such a system, for example, at couplings to momentum current (either the whole current or the two transverse components), kinetic energy density, or phase space density. We will not discuss these extensions here, though an introduction is given in Ref. [31].

[46] P. G. de Gennes, Physica A **25**, 825 (1959).

[47] J.-P. Hansen and I. R. McDonald, *Theory of Simple Liquids*, 3rd ed. (Academic Press, San Diego, CA, 2006), Chap. 3.

[48] J. K. Percus, in *The Equilibrium Theory of Classical Fluids*, edited by H. L. Frisch and J. L. Lebowitz (Benjamin, New York, 1964), pp. II–72.

[49] N. W. Ashcroft and J. Lekner, Phys. Rev. **145**, 83 (1966).

[50] One explanation for the stretched-exponential nature of the α regime is that there are many domains within the fluid each relaxing at their own rate; the observed behavior at large scale is an effective relaxation that may in fact differ markedly from the small-scale behavior within a given domain. This idea, called dynamical heterogeneity, has been seen in both experiment and simulation [4,51–54], though is not predicted by mode-coupling theory. Rather than look at the two-point density-density time correlation function we study in this work, it has been proposed that the quantity to study is the four-point correlation function relating shifted products of the density, $\rho(\mathbf{r},t)\rho(\mathbf{r}+\mathbf{r_0},t+\tau)$: $C_4(\mathbf{r},t) = \langle\delta[\rho(\mathbf{0},0)\rho(\mathbf{0}+\mathbf{r}_0,\tau)]\delta[\rho(\mathbf{r},t)\rho(\mathbf{r}+\mathbf{r}_0,t+\tau)]\rangle$. This correlation function should scale with a length ℓ which diverges at the ergodic-nonergodic transition [55–59]. While we do not address it in this paper, our theory has all the machinery necessary to study four-point quantities such as this one and could shed some light on the nature of the diverging length scale.

[51] G. Adam and J. H. Gibbs, J. Chem Phys. **43**, 139 (1965).

[52] H. Silescu, J. Non-Cryst. Solids **243**, 81 (1999).

[53] S. C. Glotzer, J. Non-Cryst. Solids **274**, 342 (2000).

[54] M. D. Ediger, Annu. Rev. Phys. Chem. **51**, 99 (2000).

[55] L. Berthier, Phys. Rev. E **69**, 020201 (2004).

[56] L. Berthier, G. Biroli, J.-P. Bouchaud, L. Cipelletti, D. El Masri, D. L'Hôte, F. Ladieu, and M. Pierno, Science **310**, 1797 (2005).

[57] G. Biroli and J.-P. Bouchaud, Europhys. Lett. **67**, 21 (2004).

[58] G. Biroli, J.-P. Bouchaud, K. Miyazaki, and D. R. Reichmann, Phys. Rev. Lett. **97**, 195701 (2006).

[59] S. Whitelam, L. Berthier, and J. P. Garrahan, Phys. Rev. Lett. **92**, 185705 (2004).

[60] R. Kohlrausch, Pogg. Ann. Phys. Chem. **91**, 179 (1854).
[61] G. Williams and D. C. Watts, Trans. Faraday Soc. **66**, 80 (1980).
[62] P. N. Pusey and W. van Megen, Nature (London) **320**, 340 (1986).
[63] Under the approximation of ignoring vertex corrections, it is possible to sum the series to all orders. Even in this extreme limit, there is little change to the transition density [33]. Full discussion of these results will be addressed elsewhere.
[64] M. Fuchs, W. Götze, I. Hofacker, and A. Latz, J. Phys. Cond. Matt. **3** (1991).
[65] T. Franosch, M. Fuchs, W. Götze, M. R. Mayr, and A. P. Singh, Phys. Rev. E **55**, 7153 (1997).
[66] A note on uncertainties: Within this paper, we will quote uncertainties estimated from the spread of values found when performing the same fit over related sets of data. This spread is generally small—signaling that the fitting forms are indeed universal, at least over the restricted sets of the fits—but it ignores the systematic uncertainty associated with our specific choices for numerical discretization. We find that there is a large phase space of choices for integration method, step size, array length, etc., that yield *good* solutions that are qualitatively identical but do show some very small quantitative differences between each other. In the absence of any *a priori* criteria to judge one set of numerical parameters better than another, we have made the most pragmatic choices. The result is that the spread in the quoted statistical uncertainty is small once we define our "numerical system" but that these uncertainties are perhaps a bit smaller than the spread in values over *all* such numerical systems for this theory. To give one example, the transition density $\eta^* = 0.60161(2)$ of Ref. [35] (Fig. 9 therein) was found via an iteration technique applied to the static equation and differs by more than one standard deviation from the transition density $\eta^* = 0.60149761(10)$ found here from the full forward-stepping dynamic solution.
[67] L. Cipelletti and E. R. Weeks, in *Dynamical Heterogeneities in Glasses, Colloids, and Granualar Media*, edited by L. Berthier, G. Biroli, J.-P. Bouchaud, L. Cipelletti, and W. Van Saarloos (Oxford University Press, Oxford, 2011), Chap. 4.
[68] J. L. Barrat, W. Götze, and A. Latz, J. Phys.: Condens. Matter **l**, 7163 (1989).
[69] L. Berthier and T. A. Witten, Phys. Rev. E **80**, 021502 (2009).
[70] A. Andreanov, G. Biroli, and J.-P. Bouchaud, Europhys. Lett. **88**, 16001 (2009).
[71] S. P. Das, G. F. Mazenko, S. Ramaswamy, and J. Toner, Phys. Rev. Lett. **54**, 118 (1985).
[72] S. P. Das and G. F. Mazenko, Phys Rev. A **34**, 2265 (1986).
[73] S. P. Das and G. F. Mazenko, Phys. Rev. E **79**, 021504 (2009).
[74] K. Kawasaki, Physica A **215**, 61 (1995).
[75] D. S. Dean, J. Phys. A **29**, L613 (1996).
[76] K. Kawasaki and S. Miyazima, Z. Phys. B: Cond. Matter **103**, 423 (1997).
[77] K. Miyazaki and D. R. Reichman, J. Phys. A: Math Gen. **38**, L343 (2005).
[78] B. Kim and K. Kawasaki, AIP Conf. Proc. **982**, 223 (2008).
[79] B. Kim, K. Kawasaki, H. Jacquin, and F. van Wijland, Phys. Rev. E **89**, 012150 (2014).
[80] G. F. Mazenko, Activated dynamics and the ergodic-nonergodic transition, arXiv:cond-mat/0609591 (2006).
[81] G. F. Mazenko, Phys. Rev. E **78**, 031123 (2008).
[82] D. D. McCowan and G. F. Mazenko, Phys. Rev. E **81**, 051106 (2010).
[83] A. Andreanov, G. Biroli, and A. Lefèvre, J. Stat. Mech. (2006) P07008.
[84] M. E. Cates and S. Ramaswamy, Phys. Rev. Lett. **96**, 135701 (2006).
[85] A. Crisanti, Nuc. Phys. B **796**, 425 (2008).
[86] G. Szamel, Phys. Rev. Lett. **90**, 228301 (2003).
[87] G. Szamel, J. Chem. Phys. **127**, 084515 (2007).
[88] G. Szamel, Prog. Theor. Exp. Phys. (2013) 012J01.
[89] A. Cavagna, Physics Reports **476**, 51 (2009).
[90] M. Mézard and G. Parisi, Phys. Rev. Lett. **82**, 747 (1999).
[91] M. Mézard and G. Parisi, J. Chem. Phys. **111**, 1076 (1999).
[92] M. Cardenas, S. Franz, and G. Parisi, J. Phys. A: Math. Gen. **31**, L163 (1998).
[93] M. Cardenas, S. Franz, and G. Parisi, J. Chem. Phys. **110**, 1726 (1999).
[94] D. El Masri, G. Brambilla, M. Pierno, G. Petekidis, A. B. Schofield, L. Berthier, and L. Cipelletti, J. Stat. Mech. (2009) P07015.
[95] W. van Megen and S. M. Underwood, Phys. Rev. E **47**, 248 (1993).
[96] W. van Megen and S. M. Underwood, Phys. Rev. E **49**, 4206 (1994).
[97] H. Vogel, Phys. Z **22**, 645 (1921).
[98] G. S. Fulcher, J. Amer. Ceram. Soc. **8**, 339 (1925).
[99] G. Tammann and W. Z. Hesse, Anorg. Allg. Chem. **156**, 245 (1926).
[100] In follow-up comments, the authors defend this interpretation against claims from two other groups [101,102]. The challengers argue – by slightly different methods – that uncertainties in the absolute density or in the polydispersity of the colloid radii lead to enough ambiguity that the data is in fact consistent with a power-law divergence over the full range, putting the transition at slightly higher density, $\eta^* \sim 0.595 - 0.6$; under this interpretation, there would be no need to claim a crossover to an "activated" range. The original authors, however, argue that their control over particle size is within reason and present counter-arguments to each claim [103,104]. The debate over the existence (or even possibility) of a crossover in colloidal particles remains active; see the following footnote for more.
[101] W. van Megen and S. R. Williams, Phys. Rev. Lett. **104**, 169601 (2010).
[102] J. Reinhardt, F. Weysser, and M. Fuchs, Phys. Rev. Lett. **105**, 199604 (2010).
[103] G. Brambilla, D. El Masri, M. Pierno, L. Berthier, L. Cipelletti, G. Petekidis, and A. Schofield, Phys. Rev. Lett. **104**, 169602 (2010).
[104] G. Brambilla, D. El Masri, M. Pierno, L. Berthier, and L. Cipelletti, Phys. Rev. Lett. **105**, 199605 (2010).
[105] There remains substantial debate as to whether or not a hard-sphere or colloidal system avoids (or is theoretically able to avoid) the power law divergence predicted by mode-coupliing theory (and our own theory, Eq. (55)) in favor of the activated exponential divergence (Eq. (64)) seen in the Brambilla work [36]. Early extensions to MCT suggests that MCT is virtually exact for colloids and the power-law should hold [72], but others point to free-volume arguments that predict

the exponential divergence with $\delta = 1$ [106]. Simulation work pre-dating Brambilla *et al*. supports exponential divergence, (possibly with $\delta > 1$) [40,107], as does some new theoretical explorations of MCT [83,84], but reasons that the power-law form should be avoided remain controversial. While there is work showing exponential divergence for granular materials approaching the limit of random close packing [108–110], there is no consensus that this dynamic arrest is equivalent to the glass-transition [69].

[106] M. H. Cohen and D. Turnbull, J. Chem. Phys. **31**, 1164 (1959).

[107] L. Berthier and W. Kob, J. Phys. Condens. Matter **19**, 205130 (2007).

[108] S. Torquato, T. M. Truskett, and P. G. Debenedetti, Phys. Rev. Lett. **84**, 2064 (2000).

[109] C. S. O'Hern, S. A. Langer, A. J. Liu, and S. R. Nagel, Phys. Rev. Lett. **88**, 075507 (2002).

[110] K. S. Schweizer, J. Chem. Phys. **127**, 164506 (2007).

[111] S. I. Henderson and W. van Megen, Phys. Rev. Lett. **80**, 877 (1998).

[112] E. Zaccarelli, C. Valeriani, E. Sanz, W. C. K. Poon, M. E. Cates, and P. N. Pusey, Phys. Rev. Lett. **103**, 135704 (2009).